# Embedded Vehicle Dynamics Aiding for USBL/INS Underwater Navigation System

Marco Morgado, Paulo Oliveira, Carlos Silvestre, and José Fernandes Vasconcelos

***Abstract*— This brief presents an embedded vehicle dynamics (VD) aiding technique to enhance position, velocity, and attitude error estimation in low-cost inertial navigation systems (INSs), with application to underwater vehicles. The model of the VD provides motion information that is complementary to the INS and, consequently, the fusion of both systems allows for a comprehensive improvement of the overall navigation system performance. In this brief, the specific VD equations of motion are directly embedded in an extended Kalman filter, as opposed to classical external vehicle models that act as secondary INSs. A tightly-coupled inverted ultrashort baseline is also adopted to enhance position and attitude estimation using measurements of relative position of a transponder located in the vehicle mission area. The improvement of the overall navigation system is assessed in simulation using a nonlinear model of the INFANTE autonomous underwater vehicle, resorting to extensive Monte Carlo runs that implement perturbed versions of the nominal dynamics. The results show that the vehicle dynamics produce relevant performance enhancements, and that the accuracy of the system is robust to modeling uncertainties.**

***Index Terms*— Inertial navigation systems, position and attitude estimation, ultrashort baseline, vehicle dynamics (VD) aiding.**

## NOMENCLATURE

Column vectors and matrices are denoted, respectively, by boldfaced lower-case and upper-case symbols, e.g., $\mathbf{y}$ and $\mathbf{Y}$. Scalar quantities are represented by lower-case regular typeface symbols, e.g., $y$. The representation $[\mathbf{y}\times]$ is the skew-symmetric matrix that denotes the cross product of $\mathbf{y} \in \mathbb{R}^3$ and $\mathbf{u} \in \mathbb{R}^3$ such that $[\mathbf{y} \times ]\mathbf{u} = \mathbf{y} \times \mathbf{u}$. The transpose of a vector or matrix will be indicated with the superscript $T$, e.g., $\mathbf{y}^T$ or $\mathbf{Y}^T$. Leading subscripts and superscripts identify the coordinate system of a quantity, e.g., ${}^E\mathbf{y}$ is represented in the earth-fixed coordinate frame and ${}^B\mathbf{y}$ is represented in the body-fixed coordinate frame. The matrix $\boldsymbol{\mathcal{R}} \in SO(3)$ is the shorthand notation for body $\{B\}$ to earth $\{E\}$ coordinate frames rotation matrix ${}^E_B\mathbf{R}$, that transforms the vector representation ${}^B\mathbf{y}$ into ${}^E\mathbf{y}$ by means of the linear operation ${}^E\mathbf{y} = {}^E_B\mathbf{R}\,{}^B\mathbf{y}$. The measurement and the estimate of quantity $\mathbf{y}$ are denoted by $\mathbf{y}_r$ and $\hat{\mathbf{y}}$, respectively. The attitude error rotation vector $\delta\boldsymbol{\lambda}$ is defined by $\tilde{\mathbf{R}}(\delta\boldsymbol{\lambda}) \triangleq \hat{\boldsymbol{\mathcal{R}}}\boldsymbol{\mathcal{R}}^T$. Position, velocity and acceleration are denoted, respectively, by $\mathbf{p}$, $\mathbf{v}$, and $\mathbf{a}$, and the angular velocity of the vehicle expressed in body-fixed coordinates by $\boldsymbol{\omega}$. The position of a transponder in earth coordinates is denoted by $\mathbf{s}$, and the transponder position in body coordinate frame is represented by $\mathbf{r}$. The superscripts $+$ and $-$ denote *a priori* information and corrected *a posteriori* quantities, respectively, e.g., $\mathbf{s}^+$ and $\mathbf{s}^-$.

Manuscript received April 18, 2011; revised December 12, 2012; accepted January 13, 2013. Manuscript received in final form January 31, 2013. This work was supported in part by the FCT under Grant PEst-OE/EEI/LA0009/2011, and Project FCT PTDC/EEA-CRO/111197/2009—MAST/AM, and the EU Project TRIDENT under Contract 248497. The work of M. Morgado was supported by the Portuguese FCT POCTI Programme, Ph.D. Student Scholarship, under Grant SFRH/BD/25368/2005. Recommended by Associate Editor A. Serrani.

M. Morgado and J. F. Vasconcelos are with the Laboratory of Robotics and Systems in Engineering and Science, Instituto Superior Técnico, Universidade Técnica de Lisboa, Lisbon 1049-001, Portugal (e-mail: marcomorgado@isr.ist.utl.pt; jfvasconcelos@isr.ist.utl.pt).

P. Oliveira is with the Department of Mechanical Engineering and with the Laboratory of Robotics and Systems in Engineering and Science, Instituto Superior Técnico, Universidade Técnica de Lisboa, Lisbon 1049-001, Portugal (e-mail: pjcro@isr.ist.utl.pt).

C. Silvestre was with the Department of Electrical Engineering and Computers, and Laboratory of Robotics and Systems in Engineering and Science, Instituto Superior Técnico, Universidade Técnica de Lisboa, Lisbon 1049-001, Portugal. He is now with the Department of Electrical and Computer Engineering, Faculty of Science and Technology, University of Macau, Macau 100872, China (e-mail: csilvestre@umac.mo).

Color versions of one or more of the figures in this paper are available online at http://ieeexplore.ieee.org.

Digital Object Identifier 10.1109/TCST.2013.2245133

## I. INTRODUCTION

THE DESIGN and implementation of navigation systems stands out as one of the most critical steps toward the successful operation of autonomous vehicles. The quality of position, velocity, and attitude estimates of the navigation system dramatically influences the capability of the vehicles to perform precision-demanding tasks. See [1] for an interesting and detailed survey on underwater vehicle navigation and its relevance. Performance degradation and limitations inherent to low-cost inertial navigation system (INSs), associated to open-loop unbounded estimation errors, unfiltered sensor noise, and uncompensated bias effects, are often tackled by merging additional information sources with nonlinear filtering techniques. Among a diverse set of techniques, an extended Kalman filter (EKF) in a direct-feedback configuration [2] is commonly adopted to estimate and compensate the INS integration error buildup. This brief addresses the merging of underwater VD information with a low-cost INS, by means of a reduced-state internal vehicle model, as opposed to classical fully-fledged external vehicle models aiding techniques, and presents an exhaustive assessment of the achievable performance improvement.

Available underwater navigation aiding sensors include Doppler velocity log (DVL), inclinometers, depth pressure sensors, magnetic compasses, whereas acoustic systems systems [3], [4], such as long baseline (LBL), short baseline (SBL), and ultrashort baseline (USBL), often stand as the primary choice for underwater positioning [5], [6]. Although long baseline-based solutions offer more information and precision, key factors, such as high-cost and time-consuming procedures

for deployment and calibration, prohibit their use in low-cost operations. Hull-mounted short baseline positioning systems, in large oceanic vessels, have to actively compensate for baseline changes due to natural bending of the hull, degrading their performance. The fast deployment, less complex hardware, and increasing performance of modern factory-calibrated ultrashort baseline positioning devices makes them suitable for faster deployment intervention missions, when compared to long baseline dependent solutions.

The development of the aforementioned navigation systems still has to bear in mind key features, such as low-cost, compactness, high performance, versatility, and robustness. The scientific community has been striving to improve low-cost navigation systems accuracy, directing much of the recent efforts toward the inclusion of VD information models in the INS [7]–[10]. The vehicle model dynamics yield unique data that provides a comprehensive set of observations of the inertial system errors, allowing for enhanced INS error compensation. Moreover, the vehicle model is a software based, passive information source valid for most operating conditions, that is not subject to interference and jamming as generic aiding sensors are, allowing for a sustainable aiding source when acoustic sensor outages occur, which is one of the most challenging issues in acoustic underwater positioning. It does require; however, additional sensor information from the vehicle actuators, i.e., fin angles, propeller rotational speed, etc., that are, nonetheless, generally available on automated vehicles for control purposes. Several approaches might be considered to include restrictions to a rigid-body motion integration algorithm: full-state complex aircraft dynamics have been adopted in [7] and [9], whereas simple nonholonomic constraints have been applied to wheeled vehicles, by setting virtual zero-velocity observations in the constrained directions [11]. Recent promising results with the HUGIN autonomous underwater vehicle (AUV) in underwater experiments validated the use of such VD aiding techniques in real-life operation scenarios [10].

In this brief, a VD model inclusion technique for underwater vehicles is presented, inspired by the embedding methodology recently proposed in [12], exploiting the specificity of the VD at hand, to extract the integration error from the generic equations of motion implemented by the INS. Classical VD aiding techniques, such as the ones adopted in [7], [9], and [10], integrate the full state VD, playing the role of a more specific secondary INS unit. These types of algorithms require additional VD errors to be estimated and properly compensated in external vehicle simulators. In the solution proposed herein, the VD are directly embedded in-the-loop, as in [12], by numerically integrating the vehicle-specific angular motion dynamics in the EKF, and extracting the necessary correction terms from the rate gyros and accelerometer data. The difference between the embedded vehicle model and classical external model aiding techniques is not addressed in this brief as this subject has been well covered in [12]. This brief is the first to extensively validate the reduced-state embedded vehicle model aiding technique presented in [12], whereas classical full-state external model techniques have been already extensively covered in the literature, see [7]–[10].

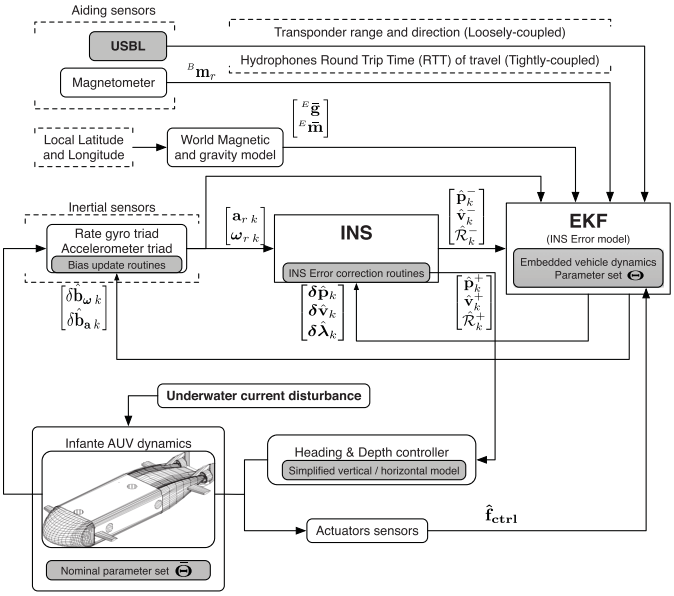


Fig. 1. Navigation system block diagram—a direct-feedback loop in which an EKF dynamically estimates the INS errors and inertial sensor biases, with the aid of external sensors and VD information—the thrusters and control surfaces are sensed and passed on to the VD embedded in the EKF.

Numerical simulation results are presented using a nonlinear model of the INFANTE AUV developed at ISR, see [13] and [14]. The performance enhancement of the proposed technique is evidenced through exhaustive Monte Carlo simulations, in which for each run the vehicle is exposed to different initial conditions, sensor noise, and the dynamics model is perturbed from the nominal plant. This brief follows preliminary work presented in [15], providing not only a more efficient way of embedding the VD as a navigation aid, but also a more detailed description of the VD, its implementation in the navigation system, and a more thorough performance analysis by considering vehicle model disturbances and underwater currents. In the considered mission scenario, the vehicle is equipped with an INS and an ultrashort baseline array in an inverted configuration [4]. For localization purposes, the vehicle interrogates transponders located in known positions of the vehicle's mission area, engaging in interrogations over considerable distances, which can vary from a few meters to several kilometers.

This brief is organized as follows. The main aspects of the navigation system and the proposed architecture are reviewed in Section II. Section III describes the ultrashort baseline system and the integration of the sensors information into the navigation system structure. The VD aiding technique is brought to full detail in Section IV, and simulation results of the overall navigation system are presented in Section V. Finally, Section VI presents conclusions and comments on future work.

## II. Navigation System Architecture

This section describes the navigation system architecture, depicted in Fig. 1, without the embedded vehicle dynamics that will be detailed later in Section IV. The INS is the backbone

system comprised by the hardware and algorithms that perform attitude, velocity, and position numerical integration from rate gyro and accelerometer triads data, rigidly mounted on the vehicle structure (strap-down configuration). The nonideal inertial sensor effects due to noise and bias are dynamically compensated and filtered, respectively, by the EKF to enhance the navigation system's performance and robustness. Position, velocity, attitude and bias compensation errors are estimated by introducing the aiding sensors data in the EKF, and are thus compensated in the INS according to the direct-feedback configuration shown in Fig. 1.

The inertial sensor readings are corrupted by zero-mean white noise $\mathbf{n}$ and random walk bias, $\dot{\mathbf{b}} = \mathbf{n}_b$, yielding

$$\mathbf{a}_r = {}^B\dot{\mathbf{v}} + \boldsymbol{\omega} \times {}^B\mathbf{v} - {}^B\mathbf{g} - \delta\hat{\mathbf{b}}_a + \mathbf{n}_a \tag{1}$$

$$\boldsymbol{\omega}_r = \boldsymbol{\omega} - \delta\hat{\mathbf{b}}_\omega + \mathbf{n}_\omega \tag{2}$$

where $\delta\hat{\mathbf{b}} = \hat{\mathbf{b}} - \mathbf{b}$ denotes bias compensation error, $\mathbf{b}$ is the nominal bias, $\hat{\mathbf{b}}$ is the estimated bias, and the subscripts $a$ and $\omega$ identify accelerometer and rate gyro quantities, respectively. For highly manoeuvrable vehicles, the INS numerical integration must properly address the angular, velocity, and position high-frequency motion effects, referred to as coning, sculling, and scrolling, respectively, to avoid estimation errors buildup. The INS multirate approach, based on the work detailed in [16] and [17], computes the dynamic angular rate/acceleration effects using high-speed, low order algorithms, whose output is periodically fed to a moderate-speed algorithm that computes attitude/velocity resorting to exact, closed-form equations. For the particular sensors and VD at hand, the high-speed algorithm and the moderate speed computations are processed at 100 and 50 times per second, respectively. Applications within the scope of this brief are characterized by confined mission scenarios and limited operational time allowing for a simplification of the frame set to earth and body frames and the use of an invariant gravity model without loss of precision. For further details on this particular navigation system structure, the reader is referred to [18] and references therein.

### A. Inertial Error Dynamics

In a standalone INS, bias and inertial sensor errors compensation is usually performed based on extensive off-line calibration procedures and data. The usage of filtering techniques in navigation systems allows for the dynamic estimation of inertial sensor nonidealities, bounding the INS errors. From the myriad of existing filtering techniques, such as particle filters, unscented Kalman filters (UKF), among others, the EKF is used in this brief to estimate and compensate the INS errors. The adopted inertial error dynamics were brought to full detail by Britting [19] and are based on perturbational rigid body kinematics. These error dynamics are applied to local navigation in confined mission areas by modeling the position, velocity, attitude, and bias compensation errors dynamics, respectively

$$\begin{aligned}
\delta\dot{\mathbf{p}} &= \delta\mathbf{v} \\
\delta\dot{\mathbf{v}} &= -\boldsymbol{\mathcal{R}}\delta\mathbf{b}_a - [\boldsymbol{\mathcal{R}}\mathbf{a}_r \times ]\delta\boldsymbol{\lambda} + \boldsymbol{\mathcal{R}}\mathbf{n}_a \\
\delta\dot{\boldsymbol{\lambda}} &= -\boldsymbol{\mathcal{R}}\delta\mathbf{b}_\omega + \boldsymbol{\mathcal{R}}\mathbf{n}_\omega \\
\delta\dot{\mathbf{b}}_a &= -\mathbf{n}_{b_a} \\
\delta\dot{\mathbf{b}}_\omega &= -\mathbf{n}_{b_\omega}
\end{aligned} \tag{3}$$

in the EKF setup in the direct-feedback configuration shown in Fig. 1. The position and velocity linear errors are defined, respectively, by

$$\delta\mathbf{p} = \hat{\mathbf{p}} - \mathbf{p} \tag{4}$$

$$\delta\mathbf{v} = \hat{\mathbf{v}} - \mathbf{v}. \tag{5}$$

The attitude error rotation vector $\delta\boldsymbol{\lambda}$, defined by $\tilde{\mathbf{R}}(\delta\boldsymbol{\lambda}) \triangleq \hat{\boldsymbol{\mathcal{R}}}\boldsymbol{\mathcal{R}}^T$, bears a first-order approximation

$$\tilde{\mathbf{R}}(\delta\boldsymbol{\lambda}) \simeq \mathbf{I}_3 + [\delta\boldsymbol{\lambda}\times] \Rightarrow [\delta\boldsymbol{\lambda}\times] \simeq \hat{\boldsymbol{\mathcal{R}}}\boldsymbol{\mathcal{R}}^T - \mathbf{I}_3 \tag{6}$$

of the direction cosine matrix (DCM) form

$${}^{B_{k-1}}_{B_k}\mathbf{R}(\boldsymbol{\xi}_k) = \mathbf{I}_3 + \frac{\sin\|\boldsymbol{\xi}_k\|}{\|\boldsymbol{\xi}_k\|}[\boldsymbol{\xi}_k\times] + \frac{1-\cos\|\boldsymbol{\xi}_k\|}{\|\boldsymbol{\xi}_k\|^2}[\boldsymbol{\xi}_k\times]^2 \tag{7}$$

where $\{B_k\}$ is the body frame at time $k$ and ${}^{B_{k-1}}_{B_k}\mathbf{R}(\boldsymbol{\xi}_k)$ is the rotation matrix from $\{B_k\}$ to $\{B_{k-1}\}$ coordinate frames, parameterized by the rotation vector $\boldsymbol{\xi}_k$ that accounts for the incremental attitude update from $\{B_{k-1}\}$ to $\{B_k\}$, as measured from the high-speed computations of the INS. In particular, the underlying filter error model (3) includes the sensor's noise characteristics directly in the covariance matrices of the EKF and allows for attitude estimation using an unconstrained, locally linear and nonsingular attitude parameterization. Once computed, the EKF error estimates are fed into the INS error correction routines as depicted in Fig. 1. The attitude estimate, $\hat{\boldsymbol{\mathcal{R}}}_k^-$, is compensated using the rotation error matrix $\tilde{\mathbf{R}}(\delta\boldsymbol{\lambda})$ definition, which yields $\hat{\boldsymbol{\mathcal{R}}}_k^+ = \tilde{\mathbf{R}}_k^T(\delta\hat{\boldsymbol{\lambda}}_k)\hat{\boldsymbol{\mathcal{R}}}_k^-$, where $\tilde{\mathbf{R}}_k^T(\delta\hat{\boldsymbol{\lambda}}_k)$ is parameterized by the rotation error vector $\delta\hat{\boldsymbol{\lambda}}_k$ according to (7). The remaining state variables are linearly compensated using

$$\begin{aligned}
\hat{\mathbf{p}}_k^+ &= \hat{\mathbf{p}}_k^- - \delta\hat{\mathbf{p}}_k, \hat{\mathbf{v}}_k^+ = \hat{\mathbf{v}}_k^- - \delta\hat{\mathbf{v}}_k \\
\hat{\mathbf{b}}_{a\ k}^+ &= \hat{\mathbf{b}}_{a\ k}^- - \delta\hat{\mathbf{b}}_{a\ k}, \hat{\mathbf{b}}_{\omega\ k}^+ = \hat{\mathbf{b}}_{\omega\ k}^- - \delta\hat{\mathbf{b}}_{\omega\ k}.
\end{aligned}$$

After the error correction procedure is completed, the EKF error estimates are reset. Therefore, linearization assumptions are kept valid and the attitude error rotation vector is stored in the $\hat{\boldsymbol{\mathcal{R}}}_k^+$ matrix, preventing attitude error estimates to fall in singular configurations. At the start of the next computation cycle ($t = t_{k+1}$), the INS attitude and velocity/position updates are performed on the corrected estimates $(\hat{\boldsymbol{\lambda}}_k^+, \hat{\mathbf{v}}_k^+, \hat{\mathbf{p}}_k^+)$.

## III. Sensor-Based Aiding

In order to tackle INS error buildup, the EKF relies on observations from external aiding sensors to accurately estimate the INS errors and correct them relying on the direct feedback mechanism presented herein. This section introduces an external aiding technique based on the ranges and range-difference-of-arrival (RDOA) measured by an ultrashort

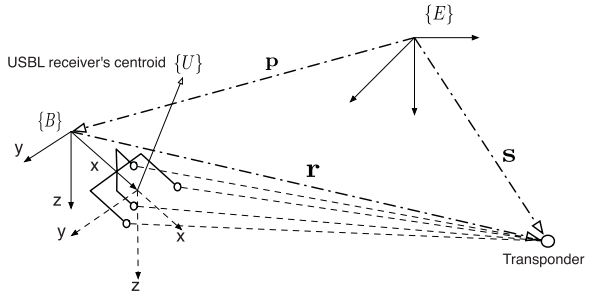


Fig. 2. Reference frames—the body-fixed coordinate frame is rigidly attached to the vehicle, while the earth reference frame is attached to a fixed point on the mission area.

baseline, installed in an inverted configuration on-board the underwater vehicle [4]. The proposed information fusion technique is based on the tightly-coupled aiding strategy proposed in [20]. Section III-A presents the equations that relate the ultrashort baseline measurements to the INS errors. Notably, the physical coupling between attitude and velocity errors, shown in (3), also enables the use of the ultrashort baseline position fixes to partially estimate attitude errors. However, as this physical attachment is invariant in the body coordinate frame, the attitude error is not fully observable solely from the rate gyros, accelerometers, and ultrashort baseline measurements.

As convincingly argued in [21] for observability analysis purposes, a GPS-only aided INS with bias estimation can be approximated by a concatenation of piece-wise time-invariant systems and, under that assumption, full observability is met by performing specific manoeuvres along the desired trajectory. Based on the observability theorem [22], and as discussed in [20], a local weak observability analysis of the system reveals that either stopped or along a straight-line path, full observability is only achieved using at least three transponders (on a nonsingular geometry) or two transponders and a magnetometer. Thus, Section III-B introduces an additional source of attitude information, drawn from the observations of the earth magnetic field provided by an on-board magnetometer. In fact, this additional observation is fundamental for the overall observability of the system, since a local weak observability analysis is sufficient to infer about the need for additional aiding sensors and/or specific manoeuvres in order to render the system observable [20].

### A. USBL

The distances between the transponder and the receivers, as illustrated in Fig. 2, can be simply written in the reference frame $\{B\}$ as $\rho_i = \|\mathbf{b}_i - \mathbf{r}\|$, where $\mathbf{b}_i \in \mathbb{R}^3$ denotes the position of the receiver in $\{B\}$. Taking into account that the position $\mathbf{r}$ in the body-fixed reference frame is given by $\mathbf{r} = \boldsymbol{\mathcal{R}}^T(\mathbf{s} - \mathbf{p})$, yields

$$\rho_{ir} = \|\mathbf{s} - \mathbf{p} - \boldsymbol{\mathcal{R}}\mathbf{b}_i\|. \tag{8}$$

The tightly-coupled ultrashort baseline/INS integration strategy exploits directly the acoustic array spatial information to calculate the distances from the transponders to each receiver on the ultrashort baseline array, and feeds this information directly into the EKF. Using the position and attitude error definitions (4) and (6), respectively, directly in (8) yields

$$\rho_{ir} = \|\mathbf{s} - \hat{\mathbf{p}} + \boldsymbol{\delta}\mathbf{p} - \hat{\boldsymbol{\mathcal{R}}}\mathbf{b}_i - [\hat{\boldsymbol{\mathcal{R}}}\mathbf{b}_i \times]\boldsymbol{\delta\lambda}\|.$$

In order to improve performance, the EKF is directly fed with a set of range measurements between the transponder and all receivers on-board, and the range-difference-of-arrival between all receivers. Alternatively the filter may be driven by one range observation and a set of independent range-difference-of-arrival measurements.

### B. Magnetometer

The magnetometer provides measurements of the earth magnetic field in body-fixed coordinates and is used in the filter as a vector observation. The extra attitude measurement is drawn from the magnetometer reading that measures the earth magnetic field in the body frame ${}^B\mathbf{m}_r = \boldsymbol{\mathcal{R}}^{\mathrm{TE}}\mathbf{m} + \mathbf{n}_m$, where ${}^E\mathbf{m}$ is the nominal earth's magnetic field vector in earth fixed coordinates, assumed known and locally constant, and $\mathbf{n}_m$ is the magnetometer measurement noise.

The vector aiding measurement residual is computed by comparing the magnetometer observation to the magnetic field estimated from the INS *a priori* attitude estimate $\hat{\boldsymbol{\mathcal{R}}}$, in earth-fixed coordinates, as

$${}^E\mathbf{z}_c = \hat{\boldsymbol{\mathcal{R}}}{}^B\mathbf{m}_r - {}^E\mathbf{m} = (\hat{\boldsymbol{\mathcal{R}}}\boldsymbol{\mathcal{R}}^T - \mathbf{I}){}^E\mathbf{m} + \hat{\boldsymbol{\mathcal{R}}}\mathbf{n}_m. \tag{9}$$

Using the attitude error approximation (6) and the properties of the cross product in (9) yields

$${}^E\mathbf{z}_c = -[{}^E\mathbf{m} \times]\boldsymbol{\delta\lambda} + \hat{\boldsymbol{\mathcal{R}}}\mathbf{n}_m.$$

## IV. Vehicle Dynamics Aiding

This section presents a brief overview of the INFANTE AUV dynamics and details the VD aiding technique, and how it is embedded in the navigation system structure. The vehicle is approximately 4.2-m long, 1.1-m wide, and 0.6-m high. Two main thrusters, fully fitted with propellers and nozzles, provide propulsion to the vehicle up to a maximum rated speed, with respect to the water, of five knots (about 2.6 m/s). For direction control, the vehicle uses six fully moving surfaces: two rudders placed in front of the nozzles, and four independent bow and stern horizontal planes as illustrated.

The dynamics model of the vehicle was brought to full detail in [13] and follows the standard notation for marine vehicles [23]. Thus, using this notation, the dynamics vector $\mathbf{q}$ that fully describes the motion of the vehicle is given by $\mathbf{q} = \left[{}^B\mathbf{v}^T \ \boldsymbol{\omega}^T\right]^T$ where ${}^B\mathbf{v} = \left[u \ v \ w\right]^T$ is the linear velocity of the vehicle with its components representing, respectively, the surge, sway and heave velocities, and $\boldsymbol{\omega} = \left[p \ q \ r\right]^T$ represents the angular velocity of the vehicle in body-fixed coordinates. The VD are given in compact form by

$$M_{\mathrm{RB}}\dot{\mathbf{q}} + C_{\mathrm{RB}}(\mathbf{q})\mathbf{q} = \boldsymbol{\tau}(\dot{\mathbf{q}}, \mathbf{q}, \boldsymbol{\mathcal{R}}, \mathbf{f}_{\mathbf{ctrl}}) \tag{10}$$

where $M_{\mathrm{RB}}$ and $C_{\mathrm{RB}}(\mathbf{q})$ denote the well known rigid body inertia matrix and matrix of Coriolis and centrifugal terms, respectively—see [13] and [23] for further details. The rotation

TABLE I
INFANTE AUV PARAMETERS

| Parameter | Nominal Value [Units] | Perturbation Value - 1$\sigma$ AWGN |
|---|---|---|
| Mass $m$ | 2234.5 [Kg] | $\pm 10$ [Kg] |
| Density $\rho$ | 1030 [Kgm$^{-3}$] | $\pm 10$ [Kgm$^{-3}$] |
| Buoyancy $B$ | 21898 [N] | $\pm 10$ [N] |
| Weight $W$ | 21898 [N] | $\pm 10$ [N] |
| Inertia matrix $I_B$ | diag(700, 1700, 2000) [Nms$^2$] | $\pm 10\mathbf{I}_3$ [Nms$^2$] |
| Center of gravity $\mathbf{p}_{\text{cg}}$ | [0, 0, 0] [m] | - |
| Center of buoyancy $\mathbf{p}_{\text{cb}}$ | [0, 0, $-0.041$] [m] | $\pm 0.1$ [mm] |
| Vehicle dynamic coefficients (45 parameters: $X_{uu}$, $X_{\text{vv}}$, $Y_{\text{uv}}$, etc., see [13]) | (described in [13]) | **Level 1:** $1\sigma =$ 3% ($2\sigma =$ 6%, $3\sigma =$ 9%)<br>**Level 2:** $1\sigma = 10\%$ ($2\sigma = 20\%$, $3\sigma = 30\%$)<br>**Level 3:** $1\sigma = 30\%$ ($2\sigma = 60\%$, $3\sigma = 90\%$) |

**Note:** About 68.27% of the Monte-Carlo realizations lie within $1\sigma$, 27.2% between $2\sigma$ and $3\sigma$, and the remaining 4.53% of the realizations beyond $3\sigma$.

matrix $\boldsymbol{\mathcal{R}}$ in (10) represents the vehicle attitude and $\boldsymbol{\tau}$ denotes the vector of external forces and moments acting on the vehicle, while the input vector $\mathbf{f_{ctrl}} = \left[\delta_{\text{bc}}, \delta_{\text{sc}}, \delta_d, \delta_r, n\right]^T$ consists, respectively, by, the common mode bow plane deflection, the common mode stern plane deflection, bow and stern differential mode deflection, deflection of the rudders and propellers rotation speed. The most relevant parameters of the INFANTE AUV are presented in Table I. The vector $\boldsymbol{\tau}(\dot{\mathbf{q}}, \mathbf{q}, \boldsymbol{\mathcal{R}}, \mathbf{f_{ctrl}})$ can be further decomposed in

$$\begin{aligned}\boldsymbol{\tau}(\dot{\mathbf{q}}, \mathbf{q}, \boldsymbol{\mathcal{R}}, \mathbf{f_{ctrl}}) = \boldsymbol{\tau}_{\text{rest}}(\boldsymbol{\mathcal{R}}) + \boldsymbol{\tau}_{\text{add}}(\dot{\mathbf{q}}, \mathbf{q}) \\ + \boldsymbol{\tau}_{\text{surf/body}}(\mathbf{q}, \mathbf{f}_{\text{ctrl}}) + \boldsymbol{\tau}_{\text{prop}}(\mathbf{q}, n)\end{aligned}$$

where $\boldsymbol{\tau}_{\text{rest}}$ represents the restoring forces and moments caused by gravity and buoyancy, $\boldsymbol{\tau}_{\text{add}}$ represents the added masses, $\boldsymbol{\tau}_{\text{surf/body}}(\mathbf{q}, \mathbf{f}_{\text{ctrl}})$ captures the effects of control surfaces deflections and hydrodynamic forces and moments acting on the vehicle structure, and $\boldsymbol{\tau}_{\text{prop}}$ denotes the forces and moments generated by the main propellers (see [13] for more thorough details on the vehicle model).

The overall dynamics of the vehicle can thus be easily written as

$$\dot{\mathbf{q}} = M_{\text{RB}}^{-1}\left(\boldsymbol{\tau}(\dot{\mathbf{q}}, \mathbf{q}, \boldsymbol{\mathcal{R}}, \mathbf{f_{ctrl}}) - C_{\text{RB}}(\mathbf{q})\mathbf{q}\right) \tag{11}$$

yielding

$$\dot{\boldsymbol{\omega}} = f_{\boldsymbol{\omega},\boldsymbol{\Theta}}(\boldsymbol{\omega}, {}^B\mathbf{v}, \boldsymbol{\mathcal{R}}, \mathbf{f_{ctrl}}) \tag{12}$$

$${}^B\dot{\mathbf{v}} = f_{v,\boldsymbol{\Theta}}(\boldsymbol{\omega}, {}^B\mathbf{v}, \boldsymbol{\mathcal{R}}, \mathbf{f_{ctrl}}) \tag{13}$$

where $\boldsymbol{\Theta}$ encompasses the knowledge of the vehicle parameters, which might be disturbed from the nominal values.

Let $\hat{\mathbf{x}} = (\hat{\mathbf{p}}, \hat{\mathbf{v}}, \hat{\boldsymbol{\omega}}, \hat{\boldsymbol{\mathcal{R}}}, \hat{\mathbf{b}}_{\mathbf{a}}, \hat{\mathbf{b}}_{\boldsymbol{\omega}})$ denote the INS state estimates. In the proposed embedded VD aiding methodology, the VD (12) and (13) are linearized about the INS state estimates, using the first-order terms of the Taylor series expansion, yielding

$$\begin{aligned}\dot{\boldsymbol{\omega}} \approx f_{\boldsymbol{\omega},\boldsymbol{\Theta}}(\hat{\boldsymbol{\omega}}, {}^B\hat{\mathbf{v}}, \hat{\boldsymbol{\mathcal{R}}}, \hat{\mathbf{f}}_{\mathbf{ctrl}}) + \left.\frac{\partial f_{\boldsymbol{\omega},\boldsymbol{\Theta}}}{\partial \boldsymbol{\omega}}\right|_{\hat{\mathbf{x}}}\left(\boldsymbol{\omega} - \hat{\boldsymbol{\omega}}\right) - \left.\frac{\partial f_{\boldsymbol{\omega},\boldsymbol{\Theta}}}{\partial \delta\boldsymbol{\lambda}}\right|_{\hat{\mathbf{x}}}\delta\boldsymbol{\lambda} \\ + \left.\frac{\partial f_{\boldsymbol{\omega},\boldsymbol{\Theta}}}{\partial {}^B\mathbf{v}}\right|_{\hat{\mathbf{x}}}\left({}^B\mathbf{v} - {}^B\hat{\mathbf{v}}\right) + \left.\frac{\partial f_{\boldsymbol{\omega},\boldsymbol{\Theta}}}{\partial \mathbf{f_{ctrl}}}\right|_{\hat{\mathbf{x}}}\left(\mathbf{f_{ctrl}} - \hat{\mathbf{f}}_{\mathbf{ctrl}}\right)\end{aligned} \tag{14}$$

and

$$\begin{aligned}{}^B\dot{\mathbf{v}} \approx f_{v,\boldsymbol{\Theta}}(\hat{\boldsymbol{\omega}}, {}^B\hat{\mathbf{v}}, \hat{\boldsymbol{\mathcal{R}}}, \hat{\mathbf{f}}_{\mathbf{ctrl}}) + \left.\frac{\partial f_{v,\boldsymbol{\Theta}}}{\partial \boldsymbol{\omega}}\right|_{\hat{\mathbf{x}}}\left(\boldsymbol{\omega} - \hat{\boldsymbol{\omega}}\right) - \left.\frac{\partial f_{v,\boldsymbol{\Theta}}}{\partial \delta\boldsymbol{\lambda}}\right|_{\hat{\mathbf{x}}}\delta\boldsymbol{\lambda} \\ + \left.\frac{\partial f_{v,\boldsymbol{\Theta}}}{\partial {}^B\mathbf{v}}\right|_{\hat{\mathbf{x}}}\left({}^B\mathbf{v} - {}^B\hat{\mathbf{v}}\right) + \left.\frac{\partial f_{v,\boldsymbol{\Theta}}}{\partial \mathbf{f_{ctrl}}}\right|_{\hat{\mathbf{x}}}\left(\mathbf{f_{ctrl}} - \hat{\mathbf{f}}_{\mathbf{ctrl}}\right).\end{aligned} \tag{15}$$

The term $\left({}^B\mathbf{v} - {}^B\hat{\mathbf{v}}\right)$ in (14) and (15) can be written as

$$\left({}^B\mathbf{v} - {}^B\hat{\mathbf{v}}\right) = \boldsymbol{\mathcal{R}}^T\mathbf{v} - \hat{\boldsymbol{\mathcal{R}}}^T\hat{\mathbf{v}}$$

which, taking into account the INS velocity and attitude errors defined, respectively, in (5) and (6), yields

$$\left({}^B\mathbf{v} - {}^B\hat{\mathbf{v}}\right) \approx -\hat{\boldsymbol{\mathcal{R}}}^T\delta\mathbf{v} - \hat{\boldsymbol{\mathcal{R}}}^T[\hat{\mathbf{v}}\times]\delta\boldsymbol{\lambda}. \tag{16}$$

Using the angular velocity error definition $\delta\boldsymbol{\omega} = \hat{\boldsymbol{\omega}} - \boldsymbol{\omega} = -\delta\mathbf{b}_{\boldsymbol{\omega}} + \mathbf{n}_{\boldsymbol{\omega}}$ and (16) in (14) and (15) gives

$$\begin{aligned}\dot{\boldsymbol{\omega}} \approx f_{\boldsymbol{\omega},\boldsymbol{\Theta}}(\hat{\boldsymbol{\omega}}, {}^B\hat{\mathbf{v}}, \hat{\boldsymbol{\mathcal{R}}}, \hat{\mathbf{f}}_{\mathbf{ctrl}}) - \left.\frac{\partial f_{\boldsymbol{\omega},\boldsymbol{\Theta}}}{\partial {}^B\mathbf{v}}\right|_{\hat{\mathbf{x}}}\hat{\boldsymbol{\mathcal{R}}}^T\delta\mathbf{v} \\ - \left(\left.\frac{\partial f_{\boldsymbol{\omega},\boldsymbol{\Theta}}}{\partial \delta\boldsymbol{\lambda}}\right|_{\hat{\mathbf{x}}} + \left.\frac{\partial f_{\boldsymbol{\omega},\boldsymbol{\Theta}}}{\partial {}^B\mathbf{v}}\right|_{\hat{\mathbf{x}}}\hat{\boldsymbol{\mathcal{R}}}^T[\hat{\mathbf{v}}\times]\right)\delta\boldsymbol{\lambda} \\ + \left.\frac{\partial f_{\boldsymbol{\omega},\boldsymbol{\Theta}}}{\partial \boldsymbol{\omega}}\right|_{\hat{\mathbf{x}}}\delta\mathbf{b}_{\boldsymbol{\omega}} - \left.\frac{\partial f_{\boldsymbol{\omega},\boldsymbol{\Theta}}}{\partial \boldsymbol{\omega}}\right|_{\hat{\mathbf{x}}}\mathbf{n}_{\boldsymbol{\omega}} + \left.\frac{\partial f_{\boldsymbol{\omega},\boldsymbol{\Theta}}}{\partial \mathbf{f_{ctrl}}}\right|_{\hat{\mathbf{x}}}\delta\mathbf{f_{ctrl}}\end{aligned} \tag{17}$$

and

$$\begin{aligned}{}^B\dot{\mathbf{v}} \approx f_{v,\boldsymbol{\Theta}}(\hat{\boldsymbol{\omega}}, {}^B\hat{\mathbf{v}}, \hat{\boldsymbol{\mathcal{R}}}, \hat{\mathbf{f}}_{\mathbf{ctrl}}) - \left.\frac{\partial f_{v,\boldsymbol{\Theta}}}{\partial {}^B\mathbf{v}}\right|_{\hat{\mathbf{x}}}\hat{\boldsymbol{\mathcal{R}}}^T\delta\mathbf{v} \\ - \left(\left.\frac{\partial f_{v,\boldsymbol{\Theta}}}{\partial \delta\boldsymbol{\lambda}}\right|_{\hat{\mathbf{x}}} + \left.\frac{\partial f_{v,\boldsymbol{\Theta}}}{\partial {}^B\mathbf{v}}\right|_{\hat{\mathbf{x}}}\hat{\boldsymbol{\mathcal{R}}}^T[\hat{\mathbf{v}}\times]\right)\delta\boldsymbol{\lambda} \\ + \left.\frac{\partial f_{v,\boldsymbol{\Theta}}}{\partial \boldsymbol{\omega}}\right|_{\hat{\mathbf{x}}}\delta\mathbf{b}_{\boldsymbol{\omega}} - \left.\frac{\partial f_{v,\boldsymbol{\Theta}}}{\partial \boldsymbol{\omega}}\right|_{\hat{\mathbf{x}}}\mathbf{n}_{\boldsymbol{\omega}} + \left.\frac{\partial f_{v,\boldsymbol{\Theta}}}{\partial \mathbf{f_{ctrl}}}\right|_{\hat{\mathbf{x}}}\delta\mathbf{f_{ctrl}}\end{aligned}$$

where $\delta\mathbf{f_{ctrl}}$ represents errors in the actuators, and can be modeled as small stochastic uncertainties to increase the navigation system robustness in real implementation scenarios.

In order to exploit the different angular motion information available from the INS and from the VD, the angular motion dynamics expressed in (17) is modeled in the EKF, while the filter is fed with the angular velocity measurement $\boldsymbol{\omega}_r$ from (2) to yield the measurement residual

$$\mathbf{z}_{\boldsymbol{\omega}} := \boldsymbol{\omega}_r - \int\dot{\boldsymbol{\omega}} = -\delta\mathbf{b}_{\boldsymbol{\omega}} + \mathbf{n}_{\boldsymbol{\omega}}. \tag{18}$$

TABLE II
SENSORS AWGN CHARACTERISTICS

| Sensor | Bias | $1\sigma$ STD |
|---|---|---|
| **Accelerometer** (Crossbow CXL02TG3) | 12 mg | 0.6 mg |
| **Rate gyro** (Silicon Sensing CRS03) | 5 deg/s | 0.05 deg/s |
| **Magnetometer** (Crossbow CXM113) | - | 60 $\mu$Gauss |
| **USBL** range | - | 0.3 m |
| **USBL** RDOA | - | 6 mm |
| **USBL** elevation and azimuth | - | 0.4 deg |

TABLE III
INITIAL ESTIMATES ERROR CHARACTERISTICS

| Initial estimate | $1\sigma$ STD |
|---|---|
| **Position** | 5 m |
| **Velocity** | 0.5 m/s |
| **Attitude** | 1 deg |

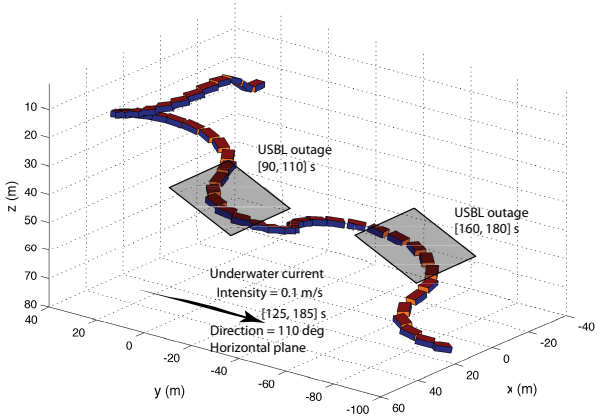


Fig. 3. Vehicle trajectory—the vehicle starts moving forward at a depth of about 10 m, and then needs to go slightly up to pitch down and dive at a constant rate while performing a snake-like trajectory.

where $\int \dot{\boldsymbol{\omega}}$ is numerically integrated in the EKF, from (12) evaluated at the estimated state $(\hat{\boldsymbol{\omega}}, {}^{B}\hat{\mathbf{v}}, \hat{\boldsymbol{\mathcal{R}}}, \hat{\mathbf{f}}_{\mathbf{ctrl}})$.

The dynamics of ${}^{B}\mathbf{v}$ expressed in (13) are used to feed the filter with the measurement residual

$$\mathbf{z}_{\mathbf{v}} := f_{v,\boldsymbol{\Theta}}(\hat{\boldsymbol{\omega}}, {}^{B}\hat{\mathbf{v}}, \hat{\boldsymbol{\mathcal{R}}}, \hat{\mathbf{f}}_{\mathbf{ctrl}}) - {}^{B}\dot{\hat{\mathbf{v}}} \tag{19}$$

where ${}^{B}\dot{\hat{\mathbf{v}}}$ is drawn from the accelerometer measurements (1) and allows for (19) to be rewritten [12] as

$$\begin{aligned}\mathbf{z}_{\mathbf{v}} = &\left([\hat{\boldsymbol{\omega}}\times] + \left.\frac{\partial f_{v,\boldsymbol{\Theta}}}{\partial {}^{B}\mathbf{v}}\right|_{\hat{\mathbf{x}}}\right)\hat{\boldsymbol{\mathcal{R}}}^{T}\delta\mathbf{v} - \left.\frac{\partial f_{v,\boldsymbol{\Theta}}}{\partial \mathbf{f}_{\mathbf{ctrl}}}\right|_{\hat{\mathbf{x}}}\delta\mathbf{f}_{\mathbf{ctrl}} + \delta\mathbf{b}_{\mathbf{a}} - \mathbf{n}_{\mathbf{a}} \\ &+ \Bigg([\hat{\boldsymbol{\omega}}\times][{}^{B}\hat{\mathbf{v}}\times] - [{}^{B}\hat{\mathbf{g}}\times] \\ &\quad + \left.\frac{\partial f_{v,\boldsymbol{\Theta}}}{\partial \delta\boldsymbol{\lambda}}\right|_{\hat{\mathbf{x}}}\hat{\boldsymbol{\mathcal{R}}} + \left.\frac{\partial f_{v,\boldsymbol{\Theta}}}{\partial {}^{B}\mathbf{v}}\right|_{\hat{\mathbf{x}}}[{}^{B}\hat{\mathbf{v}}\times]\Bigg)\hat{\boldsymbol{\mathcal{R}}}^{T}\delta\boldsymbol{\lambda} \\ &+ \left([{}^{B}\hat{\mathbf{v}}\times] - \left.\frac{\partial f_{v,\boldsymbol{\Theta}}}{\partial \boldsymbol{\omega}}\right|_{\hat{\mathbf{x}}}\right)\delta\mathbf{b}_{\boldsymbol{\omega}} + \left(\left.\frac{\partial f_{v,\boldsymbol{\Theta}}}{\partial \boldsymbol{\omega}}\right|_{\hat{\mathbf{x}}} - [{}^{B}\hat{\mathbf{v}}\times]\right)\mathbf{n}_{\boldsymbol{\omega}}.\end{aligned} \tag{20}$$

*Remark 1 (Implementation Remark):* Special care must be taken in the implementation of the VD aiding technique outlined herein, since the observation noise present in the VD measurement residuals (18) and (20) is correlated to the state noise in (3). Thus, this information about the correlation between the state and observation noise must be included in the filter implementation using modified algebraic equations for the update cycle of the EKF, as described in [24], with no additional states necessary.

## V. NUMERICAL RESULTS AND PERFORMANCE EVALUATION

The performance of the proposed VD aiding technique was assessed with the model of the INFANTE AUV. The filtering setup is exposed to extensive Monte Carlo simulations, with different initial conditions and multiple sensors noise sequences (disturbances characteristics are described in Table II and initial estimates deviations in Table III). This section presents the simulation setup, including the underwater current disturbance description, and the results analysis and discussion.

### A. Simulation Setup

The vehicle follows the trajectory depicted in Fig. 3. At time $t = 125$ s, an underwater current with an intensity of 0.1 m/s, is introduced flowing in the horizontal plane from a direction of 110 deg for 60 s. The simulation time is 200 s, which was found sufficient for the filters to achieve a steady-state behavior, that is representative of long-term operating conditions. Two 20 s periods of ultrashort baseline sensor outages are included at the intervals $t = [90, 110]$ s and $t = [160, 180]$ s. The vehicle aiding measurements and computations are processed at the same rate of the moderate speed INS computations rate, which is set to 50 Hz. The high-speed INS computations are executed at a higher rate of 100 Hz. The ultrashort baseline receiving array provides measurements once per second and is composed of four receivers that are installed on the vehicle, 30 cm away from the strap-down inertial measurement unit (IMU) setup (along the $x$-axis of the body-fixed coordinate frame $\{B\}$). Thus, the positions of the receivers with respect to $\{B\}$ are given by $\mathbf{b}_1 = [0.2\ \ -0.15\ 0]^T\ m$, $\mathbf{b}_2 = [0.2\ 0.15\ 0]^T\ m$, $\mathbf{b}_3 = [0.4\ 0\ 0.15]^T\ m$, and $\mathbf{b}_4 = [0.4\ 0\ \ -0.15]^T\ m$. The transponder is located in local inertial coordinates at ${}^{E}\mathbf{p}_t = [0\ 200\ 0]^T\ m$.

The sensors noise characteristics are summarized in Table II. The inertial sensors and magnetometers parameters are based on realistic commercially available sensor packages, and the inverted ultrashort baseline positioning system was fully developed in-house. The triaxial inertial sensors data is generated in simulation by adding the bias and additive white Gaussian noise (AWGN) described in Table II, to the data generated by the nominal VD model, and according to (1) and (2). A triaxial magnetometer is also used in the proposed solution, as described in Section III-B, which is assumed calibrated for bias, scale factors, and nonorthogonality of the input axis. The simulated magnetometer data is generated by adding the described additive white Gaussian noise to

the nominal magnetic field vector represented in the body coordinate frame (obtained as described in Section III-B and using the nominal vehicle model). Even with the addition of the external magnetic field vector observation, using only one transponder is not sufficient to obtain full state observability during straight line manoeuvres, as carefully discussed in [20]. Hence, the need for turning/diving manoeuvres built into the nominal trajectory, which is of paramount importance for observability enhancement purposes, and especially during the initial alignment phase.

Adding the corresponding additive white Gaussian noise to the nominal ranges and range-difference-of-arrival generates the ultrashort baseline data. All sensor data is generated in simulation using the vehicle model with the nominal parameter set (represented by $\bar{\Theta}$ in Fig. 1), corrupted by noise and bias. The embedded models (nonnominal or perturbed) generate the VD aiding information inside the EKF using the perturbed (nonnominal) parameter set (represented by $\Theta$ in Fig. 1 and in Section IV). Sensor modeling errors can be compensated in the filters using inflated noise [25], among other techniques, that are beyond the scope of this brief and should be assessed in experimental applications of the navigation system.

### *B. Underwater Current Disturbance*

The underwater current that disturbs the trajectory of the vehicle is assumed irrotational, such that each infinitesimal fluid element has zero angular velocity or spin (even if this current moves along a circle, i.e., changes direction over time) [10]. Under the irrotational current assumption, the vehicle model described in (11) is also valid considering water-relative velocity components [10, Property 2], that is

$$\dot{\mathbf{q}}_r = M_{\mathrm{RB}}^{-1}\left(\boldsymbol{\tau}(\dot{\mathbf{q}}_r, \mathbf{q}_r, \mathcal{R}, \mathbf{f}_{\mathbf{ctrl}}) - C_{\mathrm{RB}}(\mathbf{q}_r)\mathbf{q}_r\right) \qquad (21)$$

where $\mathbf{q}_r$ represents the linear and angular velocities of the vehicle relative to an irrotational underwater current with velocity $\mathbf{v_c} \in \mathbb{R}^3$, such that

$$\mathbf{q}_r = \mathbf{q} + [\mathbf{v_c}^T \mathcal{R} \quad \mathbf{0}_{1\times 3}]^T.$$

Note that the current velocity components related to the angular velocities of $\mathbf{q}$ are null, due to the irrotational current assumption. The expression in (21) is also valid for the zero-current case, for which $\mathbf{v_c} = \mathbf{0}_{3\times 1}$ and $\mathbf{q}_r = \mathbf{q}$. Thus, the above-mentioned underwater current disturbance in simulation is added by setting a nonzero underwater current velocity $\mathbf{v_c}$ on the right side of (21), and according to Fig. 1 before generating the simulated inertial sensors data. As illustrated in Fig. 1, the perturbed VD models that are embedded in the EKF, do not consider the underwater current disturbance.

### *C. Results Discussion*

The root-mean-square (RMS) of the position estimation error from the Monte Carlo simulations is represented in Fig. 4. The root-mean-square position estimation error results show the performance enhancement of the proposed VD aiding technique, even with the model perturbation described in Table I. The overall position performance enhancement is inherited from a comprehensive improvement of the velocity

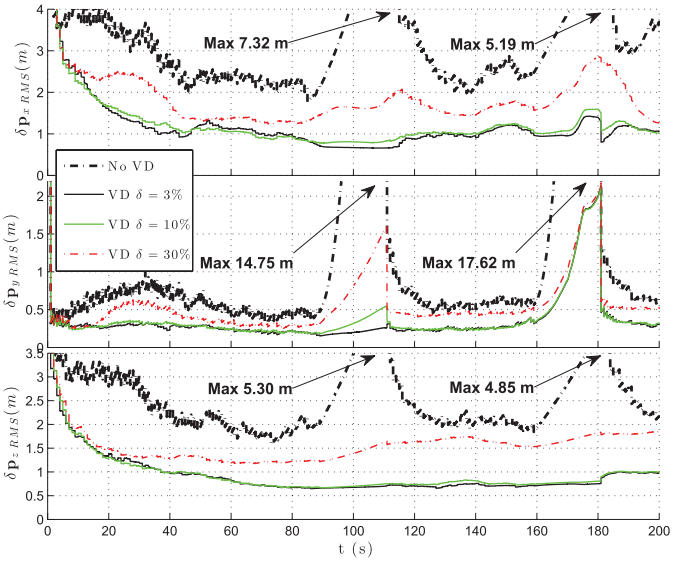


Fig. 4. Position RMS estimation error (300 Monte Carlo runs).

estimation, as the VD aiding technique provides only linear and angular velocity corrections. The enhancement on the linear velocity estimation is shown from the root-mean-square of the velocity estimation error plotted in Fig. 5. The underwater current effect in the velocity estimation error, highlighted in Fig. 5 by a grey transparent box, is more evident for the Levels 1 and 2 parameters perturbation cases. In the Level 3 case, the vehicle model parameters perturbation dominates the underwater current effect. The effect of the underwater current is also noticeable in the $y$ component of the position error drift during the ultrashort baseline outage period between 160 and 180 s. During this second outage period, all three perturbed models exhibit a similar drift in $y$ position of approximately 2 m, significantly smaller, nonetheless, than the 17.62 m drift of the VD unaided filter. During the first ultrashort baseline outage period (90 to 110 s), for which there is no underwater current, the Level 3 perturbed model aided filter exhibits a noticeable position drift that is 9 times lower than in the VD unaided case.

Overall enhancements in attitude are also achieved, as evidenced by the Monte Carlo simulations root-mean-square of the attitude estimation errors in Fig. 6. The root-mean-square estimation error for the VD filters is evidenced to be around 5 times smaller in yaw and roll, whereas a twofold reduction is obtained in pitch. Among the clear improvements in all components, the VD unaided pitch error is approximately 25 times lower than in roll in Fig. 6, due to improved observability of the overall setup for pitch estimation. The considered ultrashort baseline array-transponder geometry for the trajectory described in Fig. 3 yields reduced observability of the vehicle roll motion. Analyzing the yaw/heading root-mean-square error with VD aiding, it can be seen that the proposed system is able to achieve accuracies in the order of 0.04 deg, which is comparable to the heading accuracy of gyro-compass coupled with a state-of-the-artinertial measurement unit - around $0.02 \times \sec(lat)$ deg i.e., 0.02 deg in the equator and 0.04 deg at

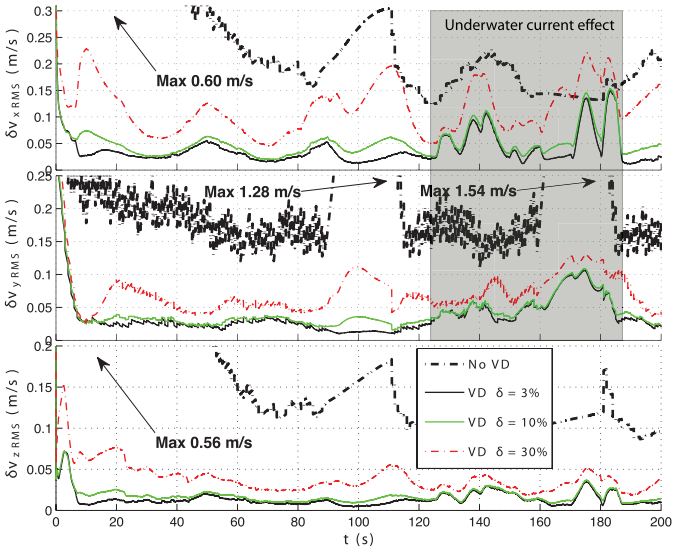


Fig. 5. Velocity RMS estimation error (300 Monte Carlo runs).

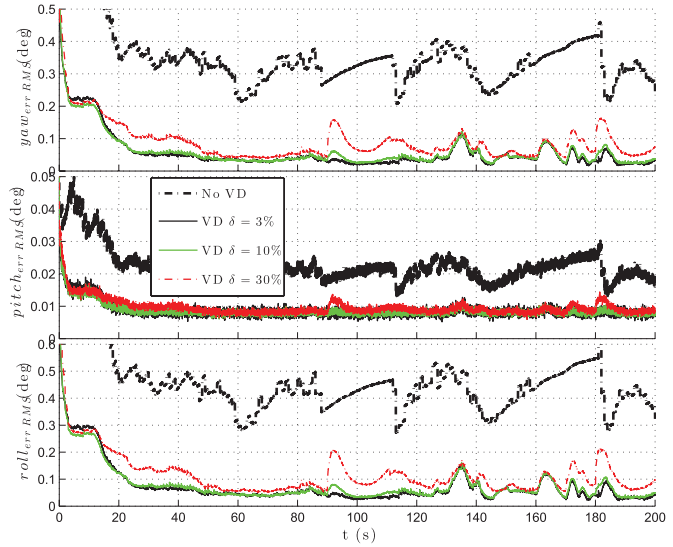


Fig. 6. Attitude RMS estimation error (300 Monte Carlo runs).

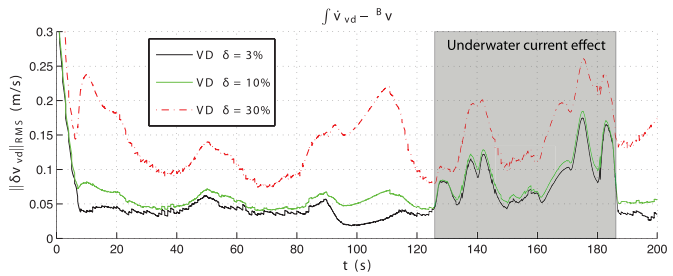


Fig. 7. Vehicle model numerically integrated linear velocity RMS error (300 Monte Carlo runs). The VD model aiding technique presented in this brief does not use this quantity, using directly linear acceleration observations drawn from the inertial sensor measurements and the linear acceleration provided by the VD model.

a latitude of ±60 deg. Despite the lack of a gyro-compass in the solution proposed herein, that level of performance is achievable due to the combination of a low-cost inertial measurement unit and three additional sources of information:

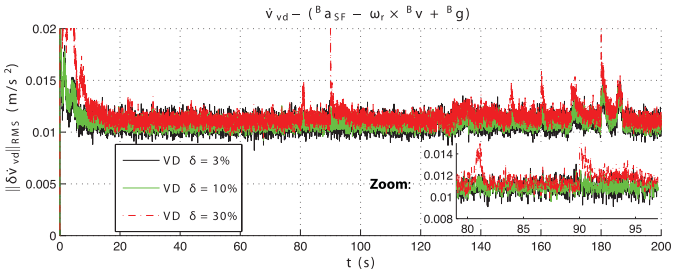


Fig. 8. Vehicle model provided linear acceleration RMS error (300 Monte Carlo runs).

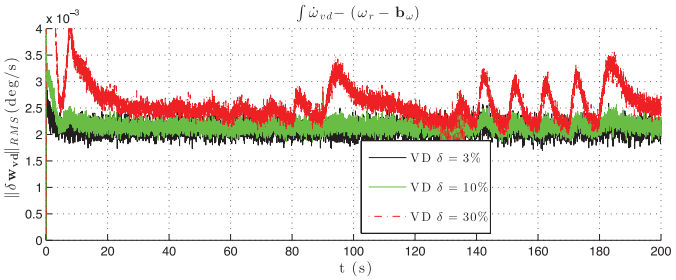


Fig. 9. Vehicle model provided angular velocity RMS error (300 Monte Carlo runs).

velocity readings from the VD model, earth magnetic field vector from the triaxial magnetometers, and ultrashort baseline position fixes. The combination of these sensors in a fully integrated package ultimately yields improved observability and attitude accuracy comparable to state-of-the-art IMU and gyro-compasses.

The linear velocity output root-mean-square error, from the considered VD perturbed models, is represented in Fig. 7, illustrating the difference between the nominal model output (with the underwater current disturbance included) and the outputs from the perturbed vehicle models. Interestingly enough, linear velocity corrections are fed directly to the filter as observations of linear acceleration drawn from the inertial sensor measurements, as given by (19), and no integration methods for the VD velocity are adopted as in classical external VD aiding techniques. Consequently, the integration of velocity aiding requires no more computational resources than those of a state update. Nonetheless, the numerical integration of the angular velocity dynamics is easily executed with an explicit fourth-order Runge–Kutta integration algorithm, making it suitable for implementation in low-power consumption hardware. The root-mean-square of the linear acceleration observations that are fed to the filters is illustrated in Fig. 8, which includes a zoom to better visualize the difference between the output root-mean-square errors of the three perturbation levels. The model-aided filter also uses the numerically integrated angular velocity from the perturbed VD models, using (18) and whose observations root-mean-square errors are illustrated in Fig. 9 for each of the VD parameters perturbation level. The information provided in Figs. 8 and 9 allows for assessing the discrepancy between the information provided by VD perturbed models and from the ground-truth information (of the nominal model) available from the on-

board sensors. Note that the filter did not diverge in any of the Monte Carlo runs, evidencing the robustness of the proposed technique under vehicle modeling errors. The performance enhancement is evident not only from the steady-state response of the filters, but also during the initial convergence phase from erroneous initial conditions.

## VI. Conclusion

An embedded VD inclusion technique was successfully adopted in this brief to enhance position, velocity, and attitude estimates of low-cost INS. The performance of the proposed VD aiding technique was assessed with the dynamics model of the INFANTE AUV, designed, and developed at IST/ISR in Lisbon, resorting to extensive Monte Carlo simulations in which the filtering setup is exposed to different initial conditions and all the sensors to different noise sequences. From the thorough results analysis of 300 Monte Carlo runs, the proposed VD aiding technique was shown to yield significantly improved performance compared to the VD unaided solution, in the presence of realistic sensor noise. The navigation system also exhibited robustness to disturbances on the vehicle model, which is a desirable feature on the practical design of navigation systems. The overall improvements in position estimation can be summarized as follows: for parameter perturbation with standard deviations of 3% and 10%, position estimation error is 2.5 times lower than in the VD unaided case, whereas for perturbations with a standard deviation of 30% the error is around 1.5 times lower than in the VD unaided case. During ultrashort baseline outages and without underwater current, the filters only revealed noticeable position drift for the perturbation Level 3, nonetheless 9 times smaller than in the VD unaided case. With the presence of underwater currents, position estimate drifts are not evident until an ultrashort baseline drop-out occurs, during which the position error drift is in line with the integration of the underwater current but still nine times less than in the VD unaided case. Enhancements in attitude estimation were likewise achieved with twofold error reduction for pitch angle estimation and fivefold for yaw and roll angles. None of the Monte Carlo runs revealed divergence of the filter, emphasizing the robustness of the proposed technique under vehicle model parameter errors (three disturbance levels with up to $1\sigma$ perturbation values of 30% in the vehicle model parameter errors). The explicit estimation of the underwater current disturbance was not addressed in this brief, in which the main contribution is centered on the validation of the embedded VD model aiding technique for underwater vehicles. Note that, on one hand, modeling the underwater current in the filter could improve filter robustness, but, on the other, it could introduce filter divergence due to modeling errors, and potential nonobservability of the augmented state space. Future work will focus on this subject and on the implementation and real-world validation of the proposed technique with an underwater vehicle.

## References


[1] J. Kinsey, R. Eustice, and L. Whitcomb, "A survey of underwater vehicle navigation: Recent advances and new challenges," in *Proc. 7th IFAC Conf. Manoeuvr. Control Marine Craft*, 2006, pp. 1–12.

[2] R. Brown and P. Hwang, *Introduction to Random Signals and Applied Kalman Filtering*, 3rd ed. New York, USA: Wiley, 1997.

[3] P. H. Milne, *Underwater Acoustic Positioning Systems*. Houston, TX, USA: Gulf, 1983.

[4] K. Vickery, "Acoustic positioning systems. new concepts—The future," in *Proc. Workshop Auto. Underwater Veh.*, Aug. 1998, pp. 103–110.

[5] X. Lurton and N. Millard, "The feasibility of a very-long baseline acoustic positioning system for AUVs," in *Proc. IEEE Oceans Eng. Today's Technol. Tomorrow's Preservat. Conf.*, vol. 3. Sep. 1994, pp. 403–408.

[6] S. Smith and D. Kronen, "Experimental results of an inexpensive short baseline acoustic positioning system for AUV navigation," in *Proc. MTS/IEEE Oceans Conf.*, vol. 1. Oct. 1997, pp. 714–720.

[7] M. Koifman and I. Y. Bar-Itzhack, "Inertial navigation system aided by aircraft dynamics," *IEEE Trans. Control Syst. Technol.*, vol. 7, no. 4, pp. 487–493, Jul. 1999.

[8] S. J. Julier and H. F. Durrant-Whyte, "On The role of process models in autonomous land vehicle navigation systems," *IEEE Trans. Robot. Autom.*, vol. 19, no. 1, pp. 1–14, Feb. 2003.

[9] M. Bryson and S. Sukkarieh, "Vehicle model aided inertial navigation for a UAV using low-cost sensors," in *Proc. Austral. Conf. Robot. Autom.*, Dec. 2004, pp. 1–9.

[10] O. Hegrenaes and O. Hallingstad, "Model-aided INS with sea current estimation for robust underwater navigation," *IEEE J. Ocean. Eng.*, vol. 36, no. 2, pp. 316–337, Apr. 2011.

[11] G. Dissanayake and S. Sukkarieh, "The aiding of a low-cost strapdown inertial measurement unit using vehicle model constraints for land vehicle application," *IEEE Trans. Robot. Autom.*, vol. 17, no. 5, pp. 731–747, Oct. 2001. X

[12] J. F. Vasconcelos, C. Silvestre, P. Oliveira, and B. Guerreiro, "Embedded UAV model and LASER aiding techniques for inertial navigation systems," *Control Eng. Pract.*, vol. 18, no. 3, pp. 262–278, Mar. 2010.

[13] C. Silvestre and A. Pascoal, "Control of the INFANTE AUV using gain scheduled static output feedback," *Control Eng. Pract.*, vol. 12, no. 12, pp. 1501–1509, Dec. 2004.

[14] C. Silvestre, R. Cunha, N. Paulino, and A. Pascoal, "A bottom-following preview controller for autonomous underwater vehicles," *IEEE Trans. Control Syst. Technol.*, vol. 17, no. 2, pp. 257–266, Mar. 2009.

[15] M. Morgado, P. Oliveira, C. Silvestre, and J. F. Vasconcelos, "Vehicle dynamics aiding technique for USBL/INS underwater navigation system," in *Proc. IFAC Conf. Control Appl. Marine Syst.*, Sep. 2007, pp. 1–6.

[16] P. Savage, "Strapdown inertial navigation integration algorithm design part 1: Attitude algorithms," *J. Guid. Control Dyn.*, vol. 21, no. 1, pp. 19–28, Jan.–Feb. 1998.

[17] P. G. Savage, "Strapdown inertial navigation integration algorithm design part 2: Velocity and position algorithms," *J. Guid. Control Dyn*, vol. 21, no. 2, pp. 208–221, Mar.–Apr. 1998.

[18] J. F. Vasconcelos, C. Silvestre, and P. Oliveira, "INS/GPS aided by frequency contents of vector observations with application to autonomous surface crafts," *IEEE. J. Ocean. Eng.*, vol. 36, no. 2, pp. 347–363, Apr. 2011.

[19] K. R. Britting, *Inertial Navigation Systems Analysis*. New York, USA: Wiley, 1971.

[20] M. Morgado, P. Oliveira, C. Silvestre, and J. F. Vasconcelos, "USBL/INS tightly-coupled integration technique for underwater vehicles," in *Proc. 9th Int. Conf. Inf. Fusion*, Jul. 2006, pp. 1–8.

[21] D. Goshen-Meskin and I. Y. Bar-Itzhack, "Observability analysis of piece-wise constant systems—Part II: Application to inertial navigation in-flight alignment," *IEEE Trans. Aerosp. Electron. Syst.*, vol. 28, no. 4, pp. 1068–1075, Oct. 1992.

[22] W. Rugh, *Linear System Theory*, 2nd ed. Englewood Cliffs, NJ, USA: Prentice-Hall, 1996.

[23] T. Fossen, *Guidance and Control of Ocean Vehicles*. New York, USA: Wiley, 1994.

[24] A. Gelb, *Applied Optimal Estimation*. Cambridge, MA, USA: MIT Press, 1974.

[25] A. H. Jazwinski, *Stochastic Processes and Filtering Theory*, vol. 64. New York, USA: Academic, 1970.